Quantitative Comparison of Two-dimensional and Three-dimensional Strain Measurement Using MRI Feature Tracking in Repair Fontan Patients and Normal Child Volunteers

Liwei Hu
Shanghai Children's Medcial Center
Qian Wang
Shanghai Children's Medical Center
Barton P Gregory
University of Wisconsin Madison
RongZhen Ouyang
Shanghai Children's Medical Center
Aimin Sun
Shanghai Children's Medical Center
Chen Guo
Shanghai Children's Medical Center
Tongtong Han
Circle Cardiovascular Imaging
Yumin Zhong (zyumin2002@163.com)
Shanghai Children's Medical Center https://orcid.org/0000-0002-0164-8752

Research article

Keywords: Strain; Feature tracking; Fontan operation; Pediatric

Posted Date: January 3rd, 2020

DOI: https://doi.org/10.21203/rs.2.11302/v3

Version of Record: A version of this preprint was published on January 28th, 2020. See the published version at https://doi.org/10.1186/s12880-020-0413-6.

Abstract

Purpose The accuracy of 2D and 3D strain analyses was evaluated by comparing strain and cardiac function parameters in Fontan repair patients and normal child volunteers. Methods We retrospectively enrolled 32 patients with Fontan circulation and 32 child volunteers who had undergone clinical cardiac magnetic resonance (CMR) assessment of the dominant ventricle with a 1.5-Tesla MRI scanner. Global and regional strain (2D and 3D) of the dominant ventricle in both groups was assessed using CMR feature-tracking. Correlations between cardiac function and strain data were assessed using Pearson's correlation coefficient values. The intraclass correlation coefficient (ICC) and coefficient of variation (CoV) were determined to evaluate repeatability and agreement. Results: The 2D GLS showed significant differences between the Fontan repair patients and volunteers (-16.49 ± 5.00 vs. -19.49 ± 2.03; p = 0.002). The 2D GRS and 2D GCS showed no significant differences between two groups. 2D GRS: 38.96 ± 14.48 vs. 37.46 ± 7.77; 2D GCS: -17.64 ± 5.00 vs. -16.89 ± 2.96, respectively; p > 0.05). The 3D global radial strain (GRS), global circumferential strain (GCS), and global longitudinal strain (GLS) showed significant differences between the Fontan repair patients and volunteers (3D GRS: 36.35 ± 16.72 vs. 44.96 ± 9.98; 3D GLS: -8.86 ± 6.84 vs. -13.67 ± 2.44; 3D GCS: -13.70 ± 7.84 vs. -18.01 ± 1.78; p < 0.05, respectively). The ejection fraction (EF) and 3D GCS were significantly associated (r = -0.491, p = 0.004). The 3D GCS showed correlations with the indexed end-diastolic volume (EDV) (r = 0.523, p = 0.002) and indexed end-systolic volume (ESV) (r = 0.602, p < 0.001). 3D strain showed good reproducibility, with GCS showing the best inter-observer agreement (ICC=0.87 and CoV=5.15), followed by GLS (ICC=0.84 and CoV=5.36). Conclusion:3D GCS is feasible, highly reproducible, and strongly correlated with conventional cardiac function measures. 3D GCS assessments may be useful for monitoring abnormal myocardial motion in patients with Fontan circulation.

Keywords Strain; Feature tracking; Fontan operation; Pediatric

Introduction

Functional single ventricle (FSV) is a type of severe congenital heart disease (CHD) [1]. The first palliation surgery for FSV was described by Fontan and Baudet [2] and performed in 1971 to treat tricuspid atresia. In patients who have undergone this Fontan repair procedure, a single ventricle provides blood flow in series to the pulmonary and systemic circulation. Young survivors with Fontan circulation commonly develop ventricular dysfunction, which has been identified as a risk factor for mortality [3, 4]. Moreover, long-term follow-up studies over the last 20 years have used echocardiography (echo) to assess ventricular function after successful Fontan surgery in childhood and shown significant differences in regional deformation and ejection fraction [5-7].

Cardiac magnetic resonance (CMR) has recently become the gold standard for measurement of ventricular function and myocardial motion [8]. CMR feature tracking (FT) has been adapted and applied to the standard CMR sequence (balanced steady-state free precession, b-SSFP) without additional sequences, unlike in myocardial tagging or displacement encoding with stimulated echoes (DENSE) imaging [9]. Strain assessment by both echo and CMR shows high intra-modality and modest inter-modality reproducibility [10]. At present, our study found that two-dimensional (2D) strain analysis is

considered a suitable tool to detect early abnormalities of the ventricular myocardium [11]. However, ventricular function assessment is challenging in post-Fontan FSV patients due to the complex ventricular geometry. Some studies have indicated that three-dimensional (3D) strain analysis may overcome such geometry-dependent limitations of 2D strain analysis by referencing the intrinsic directions of deformation [12, 13]. To our knowledge, there are no previous studies assessing three-dimensional strain analysis of SSFP cine images in Fontan patients and normal volunteers [14]. Thus, the aim of this study is to explore the feasibility of 3D strain analysis with 2D cine CMR images that may be clinically useful in the assessment of post Fontan patients.

Materials And Methods

Study Population

Our study was approved by the ethics committee of our hospital and was conducted in accordance with the Declaration of Helsinki. Thirty-two Fontan repair patients (male/female, 21/11) were retrospectively enrolled from June 2015 through August 2017. Databases were reviewed to identify patients who had undergone the Fontan procedure in infancy or early childhood (Figure 1). Then, patients who met the following criteria were retrospectively enrolled: 1) previously undergone the Fontan operation, and 2) no history of intervening surgery or catheter procedures for at least 1 year before CMR examination. The exclusion criteria were as follows: 1) presence of other diseases that could influence cardiac function in children (e.g., pulmonary hypertension, arrhythmia, valvular stenosis, or moderate to severe valvular regurgitation); 2) presence of serious liver, kidney, or lung dysfunction; and 3) inadequate image quality for analysis. Furthermore, informed consent was obtained from the parents of all the participating children. The control group consisted of 32 gender-matched healthy children with no history of cardiac disease and with LVEF ≥ 55% confirmed by echocardiography. All participants were screened using a health questionnaire and by elicitation of detailed family medical history. None of the subjects had sedation before MRI and echocardiography examination.

Cardiac Magnetic Resonance

All images were acquired using a Philips 1.5 Tesla MR Achieva system (Philips Healthcare, Best, Netherlands) with an 8-element cardiac phased array coil. Ventricular function and strain were assessed in the serial contiguous cardiac short-axis and long-axis planes (in 2- and 4-chamber views) by using a standard balanced steady-state free precession (b-SSFP) cine sequence. The parameters were as follows: repetition time (ms)/echo time (ms), 3.5/1.7; voxel size, 1.3 × 1.6 × 6-8 mm; flip angle, 60°; SENSE acceleration factor, 2.0; bandwidth, 130.8 kHz/pixel; and 20–28 phases per cardiac cycle.

Functional Analysis

Cine image analysis was performed using Circle Cardiovascular Imaging software (cvi42® version 5.6.1, Circle Cardiovascular Imaging, Canada) by two individuals with more than 10 years of experience in cardiac functional analysis who were blinded to patient demographic data. The endocardial and

epicardial borders of the dominant ventricle were manually traced on short-axis cine images at end-systole and end-diastole. Papillary muscles, trabeculae, and the rudimentary ventricle [15] were not included in FSV volumes and were excluded from the dominant ventricle mass. The ventricle end-diastolic volume (EDV), end-systolic volume (ESV), and mass were obtained from short-axis stacks. Stroke volume (SV) and ejection fraction (EF) were calculated automatically. Height and weight were measured, and body surface area (BSA) was calculated. Ventricular volume and mass were indexed to the BSA (Table 1).

Strain Analysis

The FT module was used to perform strain analysis in the patient and control groups using cvi42 software. The semi-manually defined endocardial and epicardial borders' contour at the end-diastole served as the starting point from which the software tracked displacement of spatial features in successive sequence images (Figure 2). 2D global longitudinal strain (GLS) was measured from the two- and four-chamber planes of the dominant ventricle at end-diastole, and global circumferential strain (GCS) and global radial strain (GRS) were taken from the short-axis and four-chamber planes from the basal to the apical slices. In 3D strain analysis, a 3D deformable model of the myocardium is generated in the end-diastolic phase by interpolating the endo- and epicardial boundaries tracked by the 2D algorithm (Figure 3).

Statistical Analysis

A single observer reviewed all CMR-FT studies and performed the image analyses. To assess intra-observer variability, the same investigator re-analyzed 10 random studies continuously 2 weeks after the first analysis. To evaluate inter-observer reproducibility, the same cases were then evaluated by a second observer who was blinded to the results recorded by the first observer. Intra-observer and inter-observer agreement for 2D/3D global radial, circumferential and longitudinal strain were measured using Bland Altman method by CMR with 10 random studies.

Results

Subgroup Functional Analysis

Cardiac function parameters of the 32 study subjects and 32 control children are presented in Table 1. The FSV showed a left ventricular morphology in 21 cases and a right ventricular morphology in 11 cases. The two groups showed significant differences in mean ages (9.5 ± 3.41 vs. 13.12 ± 2.87 years), mean heart rates (84 ± 21 vs. 72 ± 13 beats/min), mean BSAs (1.04 ± 0.29 vs. 1.48 ± 0.23 m^2), and ventricle mass (47.77 ± 28.81 vs. 90.40 ± 25.83 g). However, there were no statistically significant CMR volumetric differences between the groups ($p > 0.05$ for all; Table 1).

Strain Analysis

The mean GRS, GCS, and GLS (2D and 3D) values for the two groups are presented in Table 2. The 2D GLS showed significant differences between the Fontan repair patients and volunteers (-16.49 ± 5.00 vs. -19.49 ± 2.03; $p = 0.002$; Table 2). The 2D GRS and 2D GCS showed no significant differences between two groups. 2D GRS: 38.96 ± 14.48 vs. 37.46 ± 7.77; 2D GCS: -17.64 ± 5.00 vs. -16.89 ± 2.96, respectively; $p > 0.05$; Table 2). The 3D GRS, 3D GCS, and 3D GLS all showed significant differences between the Fontan repair patients and volunteers (3D GRS: 36.35 ± 16.72 vs. 44.96 ± 9.98; 3D GLS: -8.86 ± 6.84 vs. -13.67 ± 2.44; 3D GCS: -13.70 ± 7.84 vs. -18.01 ± 1.78, respectively; $p < 0.05$; Table 2).

The 2D GCS were highly correlated with cardiac function in Fontan repair patients (EF: $r = -0.612$, $p < 0.001$, EDV_i: $r = 0.471$, $p = 0.006$, ESV_i: $r = 0.556$, $p = 0.001$, Table 3) respectively. The 2D GRS have good correlation with cardiac function, (EF: $r = 0.641$, $p < 0.001$, EDV_i: $r = -0.455$, $p = 0.008$, ESV_i: $r = -0.533$, $p = 0.002$, Table 3) respectively. We also found a significant association between EF and 3D GCS ($r = -0.491$, $p = 0.004$, Table 3). The indexed EDV and ESV correlated with 3D GCS ($r = 0.523$, $p = 0.002$, $r = 0.602$, $p < 0.001$, Table 3), respectively. The mean regional circumferential strain (2D and 3D) values were compared in the Fontan repair patients. At the base, the 3D circumferential strain was higher than the 2D circumferential strain (-16.39 ± 5.63 vs. -12.67 ± 5.16, $p = 0.001$, Table 4). In the midmyocardium, 2D circumferential strain was not significantly different from 3D circumferential strain (-19.32 ± 5.00 vs. -17.86 ± 5.00, $p = 0.06$, Table 4). At the apex, the 3D circumferential strain was significantly lower than the 2D circumferential strain (-16.38 ± 4.66 vs. -22.00 ± 5.29, $p < 0.001$, Table 4).

The 2D global strain assessments showed good intra- and inter-observer agreement, except the inter-observer agreement for 2D GRS. The 3D strain showed better reproducibility than did 2D strain assessments, with GCS showing the best inter-observer agreement (ICC, 0.87 and CoV=5.15), followed by GLS (ICC 0.84 and CoV=5.36) and GRS (ICC 0.80 and CoV=10.29) (Table 5).

Discussion

The Fontan procedure is the final step in the staged palliative repair of FSV [16], and children who have undergone this procedure are at risk for clinical complications. Fontan repair patients show comparatively good preservation of ventricular function in the intermediate term; however, ventricular function deteriorates in most patients over time [17]. Ventricular dysfunction attributed to long-term volume and pressure overload could have been more prominent in the post-Fontan operation by average five-years follow-up.

Berganza et al reported that the 3D GCS was associated with the indexed right ventricular EDV in patients with repaired tetralogy of Fallot [12]. We found a strong correlation between 3D GCS and indexed EDV, indexed ESV, EF in the Fontan repair patients. Meanwhile, the 3D strain showed better reproducibility than the 2D strain in our study. 3D GCS showed the best inter-observer agreement (ICC=0.87, CoV=5.15), followed by 3D GLS (ICC=0.84, CoV=5.36) as compared to 2D GCS (ICC 0.82, CoV=5.73). Previous studies reported that CMR-FT–derived 2D GLS had the best intermodality agreement among the indices measured, followed by 2D GCS, whereas 2D GRS showed more degrees of divergence between CMR-FT

and speckle tracking echocardiography [27],[28]. Our results consistently indicated the high clinical applicability of 3D GCS and GLS as most robust parameters. In our study, the coefficient of variation of 3D GRS was not good (Figure 4). GRS represented strain throughout the entire myocardial wall from subepicardium to subendocardium and was consequently much more affected by through plane motion and complex diastolic and systolic twisting motion [29].

Our study was limited by its single-center design. The retrospective nature of the study also limited its population to those clinically referred for CMR, allowing for a potential selection bias. Due to the limitations of acquisition time, we collected SSFP cine images in the four-chamber, two-chamber, and short-axis views, and the three-chamber view was not included. Result had been affected on the 2D and 3D strain analysis without three-chamber view, this is also the limitation of retrospective study. There was evidence from previous studies that the problem of twisting motion and out of plane motion could affected using 3D strain compared with 2D algorithms. In addition, 3D images presented a substantially lower spatial and temporal resolution than their 2D counterpart. We inferred that these findings might be the reason why 3D GRS results are less stable and effective [30]. Furthermore, strain rate analysis was not included in our research because the temporal resolution of the CMR cine images was somewhat lower than what is commonly recommended for strain rate evaluation in children [30]. Further studies are needed to assess Fontan repair patients using 3D strain and 3D speckle-tracking echocardiography.

Conclusion

3D GCS is feasible, highly reproducible, and strongly correlated with conventional cardiac function measures. 3D GCS assessments may be useful for monitoring abnormal myocardial motion in patients with Fontan circulation.

Abbreviations

CMR: Cardiac magnetic resonance; ICC: Intraclass correlation coefficient; CoV: coefficient of variation; GRS: Global radial strain; GCS: Global circumferential strain; GLS: Global longitudinal strain; EF: Ejection fraction; EDV: End-diastolic volume; ESV: End-systolic volume; FSV: Functional single ventricle; CHD: Congenital heart disease; ECHO: Echocardiography; FT: Feature tracking; B-SSFP: Balanced Steady-state Free Precession; DENSE: Displacement Encoding with Stimulated Echoes; 2D: two-dimensional; 3D: three-dimensional; SV: Stroke volume; BSA: Body surface area.

Declarations

Ethics approval and consent to participate

The study was approved by the Regional ethics committee and all subjects provided written informed consent (The approval number is SCMCIRB-K2016051) The consent to participate was obtained from the

parents/guardians of the minors included in this study (minors are considered anyone under the age of 16).

Consent to publish

All subjects provided written consent for publication of this study and accompanying images.

Availability of data and materials

The datasets used and/or analysed during the current study are available from the corresponding author on reasonable request.

Competing interests

The authors declare no competing interests.

Funding

The present study was funded by National (China) Key Research and Development Program (No.2018YFB1107100, PI: YM Zhong), Shanghai Committee of Science and Technology (No.17DZ2253100, PI: LW Hu), Shanghai Municipal Commission of Health and Family Planning (No.20164Y0150, PI: LW Hu). The present study was supported by Shanghai "Rising Stars of Medical Talent" Medical Imaging Practitioner Program.

Authors' Contributions

LW Hu and YM Zhong participated in the design of the study. RZ OY and C Guo carried out image acquisition from patients and healthy volunteers. Q Wang, AM Sun and TT Han performed image and data analysis. LW Hu and GP Barton participated in statistical analysis. LW Hu and YM Zhong are preparation of the paper. All authors have contributed to final manuscript and approved it.

Acknowledgements

Not Applicable

References

[1] Wilkinson JL, Anderson RH. Anatomy of functionally single ventricle. World Journal for Pediatric and Congenital Heart Surgery. 2012;3:159–164.

[2] de Leval, MR. Evolution of the Fontan–Kreutzer procedure. Seminars in Thoracic and Cardiovascular Surgery: Pediatric Cardiac Surgery Annual. 2010;13:91–95.

[3]. Cheema A, Khalid A, Wimmer A, et al. Fragmented QRS and mortality risk in patients with left ventricular dysfunction. Circulation Arrhythmia & Electrophysiology, 2010, 3:339-344.

[4]. Piran S, Veldtman G, Siu S, et al. Heart failure and ventricular dysfunction in patients with single or systemic right ventricles. Circulation, 2002, 105: 1189-1194.

[5]. Petko C, Voges I, Schlangen J, et al. Comparison of right ventricular deformation and dyssynchrony in patients with different subtypes of hypoplastic left heart syndrome after Fontan surgery using two-dimensional speckle tracking. Cardiology in the Young, 2011, 21(6):677-683.

[6]. Mair DD, Puga FJ, Danielson GK. The Fontan procedure for tricuspid atresia: early and late results of a 25-year experience with 216 patients. Journal of the American College of Cardiology.2001;37:933-939.

[7]. Wood P W, Choy J B, Nanda N C, et al. Left ventricular ejection fraction and volumes: it depends on the imaging method. Echocardiography, 2014, 31:87–100.

[8]. Gonzalez J A, Kramer C M. Role of imaging techniques for diagnosis, prognosis and management of heart failure patients: cardiac magnetic resonance. Current heart failure reports, 2015, 12: 276-283.

[9]. Kilner P J, Geva T, Kaemmerer H, et al. Recommendations for cardiovascular magnetic resonance in adults with congenital heart disease from the respective working groups of the European Society of Cardiology. European heart journal, 2010, 31: 794-805.

[10]. Ghelani S J, Harrild D M, Gauvreau K, et al. Echocardiography and magnetic resonance imaging based strain analysis of functional single ventricles: a study of intra-and inter-modality reproducibility. The international journal of cardiovascular imaging, 2016, 32: 1113-1120.

[11]. Hu L, Sun A, Guo C, et al. Assessment of global and regional strain left ventricular in patients with preserved ejection fraction after Fontan operation using a tissue tracking technique. International Journal of Cardiovascular Imaging: 2019 35(1):153-160.

[12]. Berganza F M, de Alba C G, Özcelik N, et al. Cardiac Magnetic Resonance Feature Tracking Biventricular Two-Dimensional and Three-Dimensional strains to Evaluate Ventricular Function in Children After Repaired Tetralogy of Fallot as Compared with Healthy Children. Pediatric Cardiology, 2017, 38: 566-574.

[13]. Pedrizzetti G, Claus P, Kilner P J, et al. Principles of cardiovascular magnetic resonance feature tracking and echocardiographic speckle tracking for informed clinical use. Journal of Cardiovascular Magnetic Resonance, 2016, 18: 51.

[14]. Schuster A, Morton G, Hussain S T, et al. The intra-observer reproducibility of cardiovascular magnetic resonance myocardial feature tracking strain assessment is independent of field strength. European journal of radiology, 2013, 82: 296-301.

[15]. Secchi F, Resta E C, Di Leo G, et al. Segmentation of cardiac magnetic resonance cine images of single ventricle: including or excluding the accessorial ventricle?. The international journal of cardiovascular imaging, 2014, 30: 1117-1124.

[16]. Edwards R M, Reddy G P, Kicska G. The functional single ventricle: how imaging guides treatment. Clinical Imaging, 2016, 40: 1146-1155.

[17]. Veldtman G R, Nishimoto A, Siu S, et al. The Fontan procedure in adults. Heart, 2001, 86: 330-335.

[18]. Kutty S, Rangamani S, Venkataraman J, et al. Reduced global longitudinal and radial strain with normal left ventricular ejection fraction late after effective repair of aortic coarctation: a CMR feature tracking study. The international journal of cardiovascular imaging, 2013, 29: 141-150.

[19]. Tutarel O, Orwat S, Radke R M, et al. Assessment of myocardial function using MRI-based feature tracking in adults after atrial repair of transposition of the great arteries: Reference values and clinical utility. International Journal of Cardiology, 2016, 220: 246-250.

[20] Satriano A, Heydari B, Narous M, et al. Clinical feasibility and validation of 3D principal strain analysis from cine MRI: comparison to 2D strain by MRI and 3D speckle tracking echocardiography. The international journal of cardiovascular imaging,2017,33(12):1979–1992

[21] Gatti M, Palmisano A, Faletti R,et al. Two-dimensional and three-dimensional cardiac magnetic resonance feature-tracking myocardial strain analysis in acute myocarditis patients with preserved ejection fraction. The International Journal of Cardiovascular Imaging, 2019;35(6):1101-1109.

[22]. Liu B , Dardeer A M , Moody W E , et al. Reference ranges for three-dimensional feature tracking cardiac magnetic resonance: comparison with two-dimensional methodology and relevance of age and gender. International Journal of Cardiovascular Imaging, 2018, 34(5):761-775.

[23]. André F, Robbers-Visser D, Helling-Bakki A, et al. Quantification of myocardial deformation in children by cardiovascular magnetic resonance feature tracking: determination of reference values for left ventricular strain and strain rate. Journal of Cardiovascular Magnetic Resonance, 2016, 19: 8.

[24]. Schuster A, Hor K N, Kowallick J T, et al. Cardiovascular Magnetic Resonance Myocardial Feature Tracking: Concepts and Clinical Applications. Circulation Cardiovascular Imaging, 2016, 9(4):e004077.

[25]. Satriano A , Heydari B , Narous M , et al. Clinical feasibility and validation of 3D principal strain analysis from cine MRI: comparison to 2D strain by MRI and 3D speckle tracking echocardiography. International Journal of Cardiovascular Imaging, 2017, 33(12):1979-1992.

[26]. Liu B, Sinha A, Moody W, et al. New normal ranges and superior reproducibility of 3d myocardial strain on cardiovascular magnetic resonance-feature tracking. Heart, 2017, 103(Suppl 5):A82-A83.

[27] Schuster A, Stahnke VC, Unterberg-Buchwald C, et al. Cardiovascular magnetic resonance feature-tracking assessment of myocardial mechanics: inter vendor agreement and considerations regarding reproducibility. Clinical Radiology. 2015;70:989-998.

[28]. Schuster A, Paul M, Bettencourt N, et al. Cardiovascular magnetic resonance myocardial feature tracking for quantitative viability assessment in ischemic cardiomyopathy[J]. International Journal of Cardiology, 2013, 166(2):413-420.

[29]. Gertz, R J, Lange T, Kowallick J T, et al. Inter-vendor reproducibility of left and right ventricular cardiovascular magnetic resonance myocardial feature-tracking[J]. PLoS ONE, 2018, 14;13(3):e0193746.

[30]. Zhu T, Zeng W, Chen Y, et al. 2D/3D CMR tissue tracking versus CMR tagging in the assessment of spontaneous T2DM rhesus monkeys with isolated diastolic dysfunction. BMC medical imaging 2018, 18(1): 47

[30]. Amzulescu M S, De Craene M, Langet H, et al. Myocardial strain imaging: review of general principles, validation, and sources of discrepancies[J]. European Heart Journal - Cardiovascular Imaging, 2019(0),1-15.

Tables

Table 1. CMR measurements for the patient and control groups (mean ± SD)

Variables	Patient Group (n = 32)	Control Group (n = 32)	*p* value
Age at CMR (years)	9.5 ± 3.41	13.12 ± 2.87	**<0.001**
Males (%)	21 (65%)	21 (65%)	-
Post-surgery follow-up time (years)	5.06 ± 2.24	—	-
Heart rate (beats/min)	84 ± 21	72 ± 13	0.025
Body surface area (m^2)	1.04 ± 0.29	1.48 ± 0.23	**<0.001**
EDV_i (ml/m^2)	76.21 ± 44.75	75.15 ± 10.98	0.903
ESV_i (ml/m^2)	34.40 ± 26.09	28.92 ± 6.46	0.536
$Stroke\ volume_i$ (ml)	43.25 ± 21.49	46.22 ± 7.84	0.210
Ejection fraction	58.85 ± 10.67	61.56 ± 6.03	0.138
$Ventricle\ mass_i$ (g)	47.77 ± 28.81	90.40 ± 25.83	**0.003**
SBP (mm Hg)	112 ± 8	115 ± 7	-
DBP (mm Hg)	67 ± 6	67 ± 6	-

i: indexed

There were statistical differences in bold representation

Table 2. 2D and 3D global radial, circumferential, and longitudinal strain in the patient and control groups

Variables	Patient Group (n = 32)	Control Group (n = 32)	*p* value
Radial			
2D strain	38.96 ± 14.48	37.46 ± 7.77	0.567
3D strain	36.35 ± 16.72	44.96 ± 9.98	**0.010**
Longitudinal			
2D strain	-16.49 ± 5.00	-19.49 ± 2.03	**0.002**
3D strain	-8.86 ± 6.84	-13.67 ± 2.44	**<0.001**
Circumferential			
2D strain	-17.64 ± 5.00	-16.89 ± 2.96	0.440
3D strain	-13.70 ± 7.84	-18.01 ± 1.78	**0.003**

There were statistical differences in bold representation

Table 3. Correlation between cardiac function and global strain in the patient group

Cardiac function	Strain parameter	*R*	*P*
EDV_i（ml/m^2）	2D GLS	0.312	0.082
	2D GCS	0.471	**0.006**
	2D GRS	-0.455	**0.008**
	3D GLS	0.103	0.572
	3D GCS	0.523	**0.002**
	3D GRS	-0.133	0.467
ESV_i（ml/m^2）	2D GLS	0.455	0.008
	2D GCS	0.556	**0.001**
	2D GRS	-0.533	**0.002**
	3D GLS	0.212	0.245
	3D GCS	0.602	**<0.001**
	3D GRS	-0.200	0.272
EF（%）	2D GLS	-0.539	0.001
	2D GCS	-0.612	**<0.001**
	2D GRS	0.641	**<0.001**
	3D GLS	-0.478	0.005
	3D GCS	-0.491	**0.004**
	3D GRS	0.347	0.05

i: indexed

There were statistical differences in bold representation

Table 4. Comparison of 2D and 3D regional strain in the Fontan repair groups

(n = 32)	2D Strain	3D Strain	*p* value
Circumferential			
Basal	-12.67 ± 5.16	-16.39 ± 5.63	**0.001**
Mid	-19.32 ± 5.00	-17.86 ± 5.00	0.06
Apical	-22.00 ± 5.29	-16.38 ± 4.66	**<0.001**

There were statistical differences in bold representation

Table 5. Intra-observer and inter-observer variability of CMR for 2D and 3D global strain in randomly selected 10 cases from patients with Fontan repair and controls

Variables	Intra-observer (n = 10)		Inter-observer (n = 10)	
	ICC (%)	CoV	ICC (%)	CoV
2D GLS (%)	0.91(0.84-0.94)	3.13	0.84(0.76-0.89)	5.12
2D GCS (%)	0.86(0.78-0.90)	4.92	0.82(0.73-0.88)	5.73
2D GRS (%)	0.88(0.80-0.93)	7.18	0.76(0.62-0.85)	11.23
3D GLS (%)	0.83(0.76-0.88)	3.62	0.84(0.74-0.86)	5.36
3D GCS (%)	0.89(0.83-0.92)	4.59	0.87(0.79-0.94)	5.15
3D GRS (%)	0.81(0.72-0.87)	8.17	0.80(0.67-0.88)	10.29

Figures

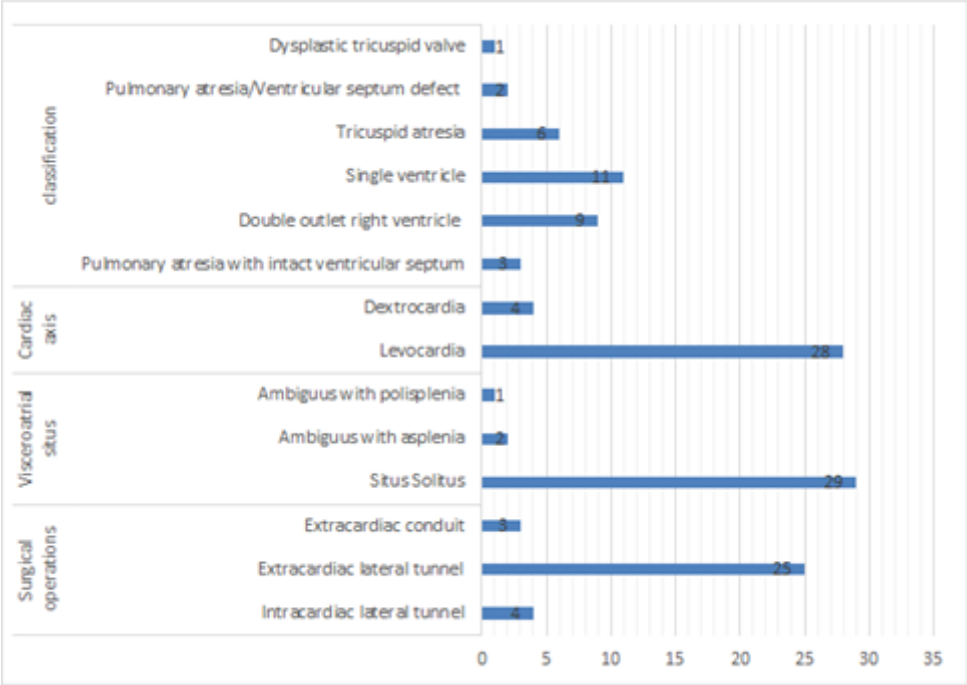

Figure 1

The clinical and diagnostic information in repaired Fontan patients

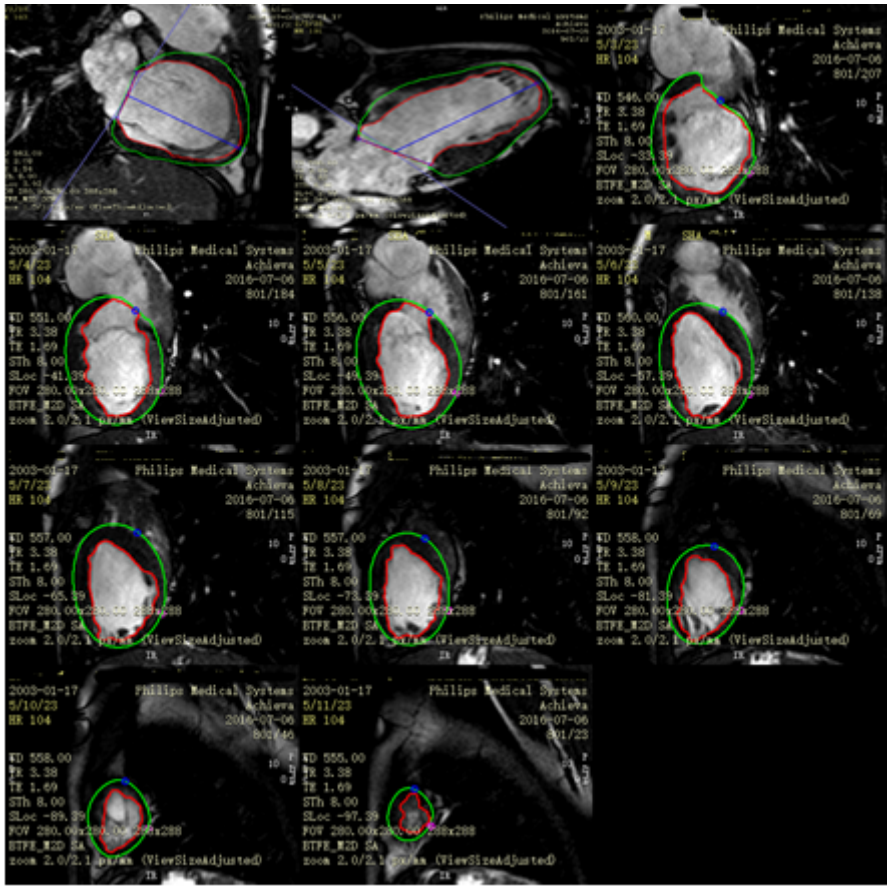

Figure 2

2D global longitudinal strain and global circumferential strain and global radial strain were taken from the short-axis and four-chamber planes from basal to apical slices at end-diastole in the post-Fontan patient case. (endocardial: red line; epicardial borders: green circle)

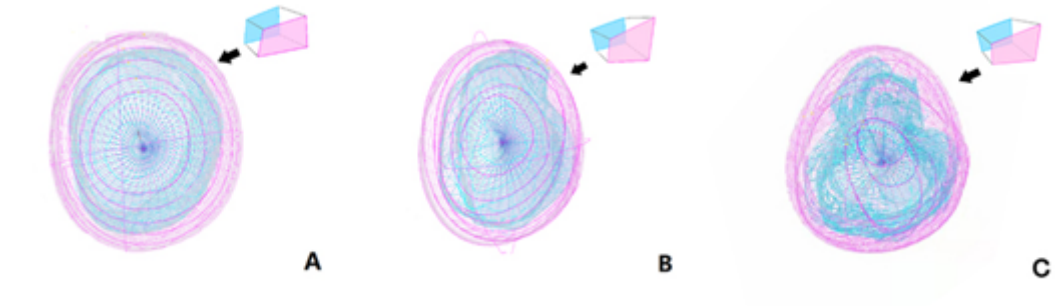

Figure 3

Figure A show 3D mesh model of volunteer; Figure B show 3D mesh map of single left ventricular morphology; Figure C show 3D mesh map of single right ventricular morphology. This mesh model was corresponding points (nodes) from respective endocardial and epicardial surfaces coupled to obtain a hexahedral 3D mesh based on a deformable model. Deformations for each hexahedral element were then calculated using a Lagrangian strain definition.

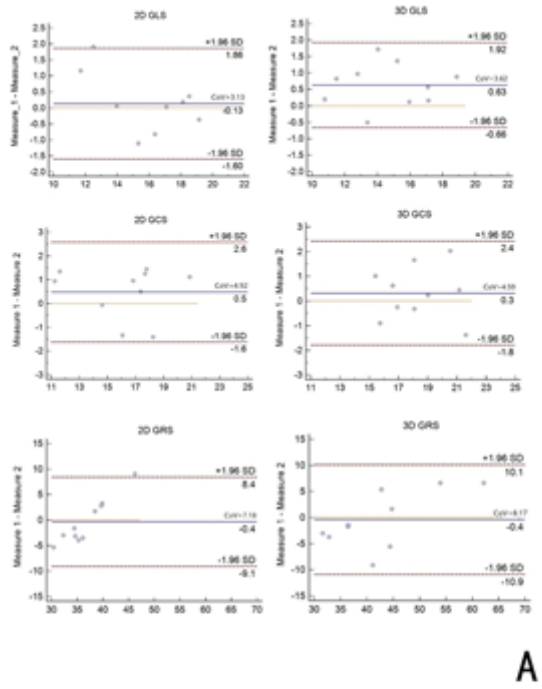

Figure 4

Intra-observer(A) and inter-observer agreement(B) for 2D/3D global radial, circumferential and longitudinal strain measurement by CMR with 10 random studies. Solid line indicated perfect agreement, dotted line indicated mean difference, dashed lines indicated 95% limits of agreement.